

Free Energy Determinants of Binding the rRNA Substrate and Small Ligands to Ricin A-Chain

Mark A. Olson and Lilee Cuff

Molecular Modeling Laboratory and Department of Cell Biology and Biochemistry, United States Army Medical Research Institute of Infectious Diseases, Frederick, Maryland 21702 USA

ABSTRACT A continuum model is provided of the free energy terms that contribute to the molecular association of ricin A-chain (RTA) with the rRNA substrate and several small ligands. The model for RTA interactions with the RNA was taken from a previously proposed complex containing a 29-mer oligonucleotide hairpin (Olson, 1997. *Proteins* 27:80–95), and models for the ligands were constructed from x-ray crystallographic structures. The calculated absolute free energies of complex formation for the RTA-RNA assembly and several single-residue substitutions are in good agreement with experimental data, given the approximations of evaluating the strain energy and conformational entropy. The free energy terms were found to resemble those of protein-protein complexes, with the net unfavorable electrostatic contribution offset by the favorable nonspecific hydrophobic effect. Decomposition of the RTA-RNA binding free energy into individual contributions revealed the electrostatic “hot” spots arising from charge-charge complementarity of the interfacial arginines with the RNA phosphate backbone. Base interactions of the GAGA loop structure dominate the hydrophobic complementarity. A linear-scaling model was parametrized for evaluating the binding of small ligands against the rRNA substrate and illustrates the free energy determinant required for designing specific RTA inhibitors.

INTRODUCTION

Ribosome-inactivating proteins (RIPs) are a large family of *N*-glycosidases that exhibit exquisite specificity in their catalytic hydrolysis of a single adenine base from among nearly 7000 nucleotides found in mammalian ribosomes. Depurination occurs at the first adenine in the loop sequence GAGA, located in a highly conserved, single-stranded rRNA hairpin. Included among the RIPs is the extraordinarily toxic ricin protein. Isolated from the seeds of the castor bean plant *Ricinus communis*, ricin is a globular heterodimer consisting of a 267-residue catalytic A-chain (RTA) linked by a disulfide bond to the cell-surface binding B-chain of 262 residues. Molecular recognition of the catalytic adenine can be inferred from x-ray crystallographic structures of RTA complexed with substrate analogs (Monzingo and Robertus, 1992). The putative adenine binding mode consists of a combination of specific hydrogen bonds and aromatic stacking between two invariant tyrosine side chains in the enzyme specificity site. Available are site-directed mutagenesis studies elucidating structure-function correlates of ricin (Day et al., 1996; Kim and Robertus, 1992; Ready et al., 1991; Frankel et al., 1990).

Owing to the remarkable cytotoxicity of ricin, there is considerable interest in the search for strong competitive inhibitors, yet only modest success has been achieved to date for small molecules (Yan et al., 1997). There is more promise for a transition-state mimic containing a modified

14-mer ribonucleotide hairpin (Chen et al., 1996), though its molecular size limits its practical use as a therapeutic inhibitor. The failure of smaller similar ribonucleotide loops to inhibit ricin (Link et al., 1995) indicates that many issues remain to be clarified regarding ligand size requirements for inhibition. Questions arise as to what interactions are critical for the substrate remote from the catalytic adenine recognition site and, more importantly, whether small molecules can effectively block the strong binding of RTA to an extended rRNA substrate.

To better understand the structural interactions between ricin and the rRNA substrate, a modeled complex was recently developed (Olson, 1997) by molecular docking the RTA crystal structure with a 29-mer oligonucleotide hairpin obtained from an NMR solution structure (Szewczak and Moore, 1995; Szewczak et al., 1993). This particular oligonucleotide contains the GAGA loop sequence and is depurinated by RTA. Conformational sampling of docking the two structures was performed by using a molecular dynamics (MD) simulated-annealing method. The calculations generated a large ensemble of complex configurational states and their analysis revealed a vast network of interactions between the two molecules, mediated by an array of contact sites arising from a group of arginines. To make the connection with experimental binding data, this paper extends the previous study by analyzing the free energy determinants of complex formation for RTA interactions with the RNA and several small ligand molecules.

We report the results of a continuum model developed for estimating macromolecular interactions in solution. Electrostatic free energies were evaluated by solving the nonlinear Poisson-Boltzmann (NLPB) equation (Reiner and Radke, 1990; Sharp and Honig, 1990), and a free-energy relationship based on the molecular surface area was used for

Received for publication 31 July 1998 and in final form 5 October 1998.

Address reprint requests to Dr. Mark A. Olson, Molecular Modeling Laboratory, USAMRIID, Department of Cell Biology and Biochemistry, 1425 Porter Street, Frederick, MD 21702. Tel.: 301-619-4236; Fax: 301-619-2348; E-mail: molson@ncifcrf.gov.

© 1999 by the Biophysical Society

0006-3495/99/01/28/12 \$2.00

modeling the hydrophobic effects (Jackson and Sternberg, 1994). A comparison of the free energies for both the RTA-RNA assembly and several protein mutants with experimentally determined affinities is presented and provides confidence in the overall validity of the modeled complex. We also present the binding free energy for the RTA-RNA complex dissected into individual contributions of protein residues and RNA nucleotides. Understanding these module or group free energies reveals the binding “signature” (or “fingerprints”; Muegge et al., 1997) of the interfacial surface, and allows for a computationally tractable assessment of the structural and functional features critical for molecular association with the rRNA substrate. Also reported are free energy terms for the small ligands in their crystallographic assemblies. Their contrast with the substrate yields insight into the difficulties encountered in designing small effective inhibitors against RTA. The paper concludes with a linear-scaling model that combines the substrate and small ligands into a single continuum framework that should prove useful in gauging the binding free energies of novel inhibitors found either by de novo design methods or database searching.

METHODS

The numerical determination of the binding free energies (ΔG_{bind}) for the RTA-RNA complex is based on the calculational approach where molecular association is partitioned into independent contributions arising from electrostatic (ΔG_{ele}) and nonpolar (ΔG_{np}) interactions, plus a strain-energy (ΔG_{strain}) and conformational entropy ($T\Delta S$) term (Gilson and Honig, 1988; Jackson and Sternberg, 1995; Froloff et al., 1997)

$$\Delta G_{\text{bind}} = \Delta G_{\text{ele}} + \Delta G_{\text{np}} + \Delta G_{\text{strain}} - T\Delta S, \quad (1)$$

where $T\Delta S$ combines the terms of side-chain torsional and translational-rotational entropy, and T is the absolute temperature. To calculate the total electrostatic free energy of the system, we used a thermodynamic pathway of association where ΔG_{ele} is expressed as a sum of three terms (Gilson and Honig, 1988)

$$\Delta G_{\text{ele}} = \Delta\Delta G_{\text{sol}}^{\text{prot-RNA}} + \Delta\Delta G_{\text{sol}}^{\text{RNA-prot}} + \Delta G_{\text{int}}^{\text{prot-RNA}} \quad (2)$$

$$\approx \int \rho \phi dv,$$

where $\Delta\Delta G_{\text{sol}}^{\text{prot-RNA}}$ corresponds to the loss of charge-solvent interaction energy through the partial desolvation of the electrostatically charged protein on binding; $\Delta\Delta G_{\text{sol}}^{\text{RNA-prot}}$ is the loss of charge-solvent interaction energy through the partial desolvation of the RNA on binding; and the term $\Delta G_{\text{int}}^{\text{prot-RNA}}$ is the electrostatic interaction energy between the two macromolecules embedded in the solvent dielectric continuum. The desolvation energetics are evaluated from the differences (Gilson and Honig, 1988):

$$\Delta\Delta G_{\text{sol}}^{\text{prot-RNA}} = \Delta G_{\text{sol}}^{\text{prot-RNA}} - \Delta G_{\text{sol}}^{\text{prot}} \quad (3a)$$

$$\Delta\Delta G_{\text{sol}}^{\text{RNA-prot}} = \Delta G_{\text{sol}}^{\text{RNA-prot}} - \Delta G_{\text{sol}}^{\text{RNA}}, \quad (3b)$$

where the reaction fields for $\Delta G_{\text{sol}}^{\text{prot-RNA}}$ and $\Delta G_{\text{sol}}^{\text{RNA-prot}}$ are determined by setting the atomic charges for the binding partner to zero. This is accomplished by using a charging cycle similar to that introduced by Lee et al. (1992). The electrostatic association process involves the removal of the high dielectric solvent (ϵ_s) from the space occupied by the binding partner and replacing it with the low dielectric medium of the macromolecule (ϵ_m).

The sum of electrostatic free energy terms in Eq. 2 is given by the volume integral of the fixed charge density, ρ , and the potential, ϕ , where the potential is evaluated from the NLPB equation (Reiner and Radke, 1990; Sharp and Honig, 1990):

$$\nabla \cdot [\epsilon(\mathbf{r}) \nabla \cdot \phi(\mathbf{r})] - \epsilon(\mathbf{r}) \kappa(\mathbf{r})^2 \sinh[\phi(\mathbf{r})] + 4\pi\rho(\mathbf{r}) = 0, \quad (4)$$

where κ is a function of the Debye length and ionic strength of the bulk solution, and \mathbf{r} is the position vector in the reference frame centered on the protein-RNA complex. Equation 4 is typically solved by the finite-difference procedure (Nicholls and Honig, 1991; Jayaram et al., 1989; Gilson et al., 1988), where the spatially dependent properties are mapped onto a cubic lattice. By using this numerical scheme we evaluated the pair-wise Coulombic interaction from the expression (Gilson and Honig, 1988; Jackson and Sternberg, 1995; Froloff et al., 1997)

$$\Delta G_{\text{int}}^{\text{prot-RNA}} = \sum_{i=1}^N q_i \phi_i, \quad (5)$$

where q_i is the charge of the bound RNA at a particular lattice point in space and ϕ_i is the potential generated by the protein at this point.

Atomic coordinates for the RTA-RNA complex were taken from a previously reported MD simulated-annealing study of docking RTA with the 29-mer RNA molecule (Olson, 1997). The RNA sequence is displayed in Fig. 1 *a*, where the adenine depurinated by RTA is designated as A15. Single-residue mutants Y80F, N209S, and R180Q were constructed from the wild-type complex by replacing the native side chains with the most favorable substituted conformers. Partial atomic charges for the protein and RNA were derived from the AMBER force field (Weiner et al., 1986). For the mutant R180Q, conformational relaxation of the phosphoribose backbone centered around A15 and G16 was performed by using a short energy minimization calculation (100 cycles using a steepest descent algorithm) and an MD simulation (1000 iterations at a temperature of 300 K using a timestep of 1 fs). The catalytic water in the RTA-RNA complex (Olson, 1997) was treated explicitly by using the TIP3P model (Jorgensen et al., 1983). Force-field cutoffs were set at 12 Å and a dielectric constant of $\epsilon = 1$ was implemented.

The DelPhi software package (Gilson et al., 1988) was used to solve Eq. 4. The complexes and the surrounding solvent were mapped onto a 173^3 lattice. Water-accessible surfaces of the macromolecules were constructed by using a 1.4-Å-radius probe to define regions of the low dielectric medium (modeled using ϵ_m values in the range of 2 to ~ 7), embedded in a dielectric solvent water ($\epsilon_s = 80$). An ion exclusion radius of 2.0 Å was added to the surfaces to account for ion size. Parameters defining atomic radii were taken from the CFF91 molecular mechanics force field (Maple et al., 1994). The ionic strength was set at physiological conditions of 0.145 M. Ionization states for residues Asp, Glu, Lys, Arg, and His were set corresponding to a neutral pH. Full Coulombic boundary conditions were applied for all calculations and the number of nonlinear iterations for solving the NLPB equation was set at 250. Dummy atoms were used to retain an identical scale and position on the grid for the complexes and individual structures. Systematic errors were estimated to be $<2\%$ when compared with calculations carried out with increased grid resolutions. Calculational dependencies of the results on the position of the molecule on the grid were acceptably small and, therefore, neglected.

Atomic coordinates for ligands pteric acid (PTA), formycin 5'-monophosphate (FMP), and adenylyl-3',5'-guanosine (ApG) bound to the RTA protein were kindly provided by Dr. Jon Robertus (Yan et al., 1997; Monzingo and Robertus, 1992). Chemical formulas for PTA and FMP are illustrated in Fig. 1, *b* and *c*, with hydrogens added according to the suggested PTA structure (Yan et al., 1997, 1998) and from previous modeling calculations of FMP (Olson et al., 1995). The phosphate group of FMP was modeled either as a monoanion or dianion. Charges for the ligand-bound proteins were the same as the RTA-RNA complex, while those of PTA and FMP were derived from ab initio quantum mechanical calculations by using the 6-31g** basis set. For the dinucleotide ApG,

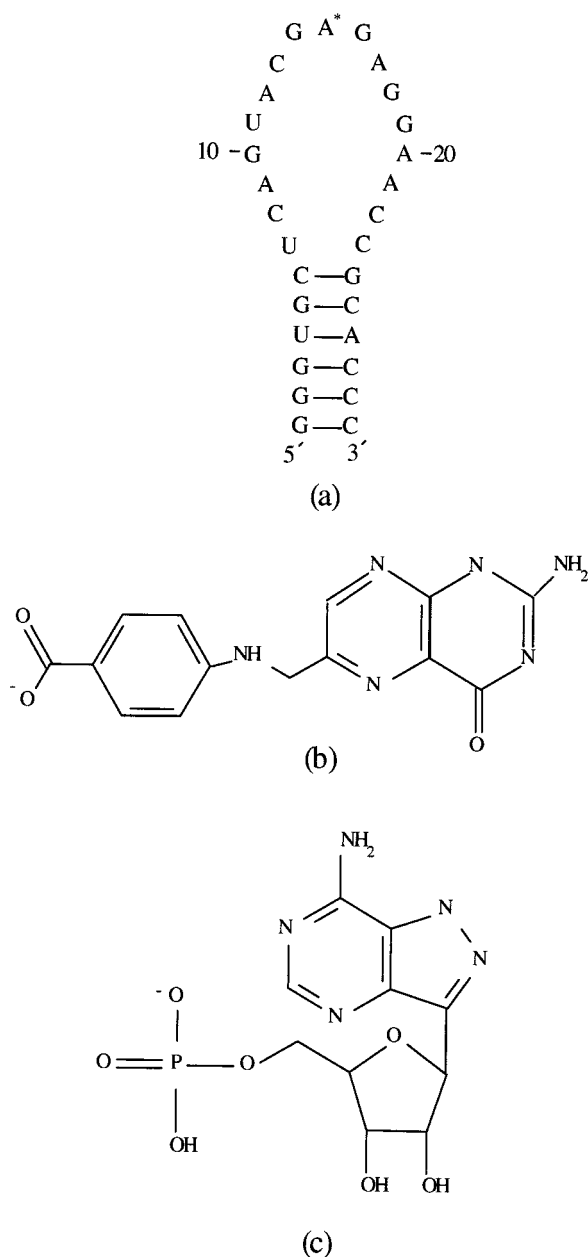


FIGURE 1 (a) RNA sequence of the 29-mer oligonucleotide hairpin where the target adenine for ricin A-chain depurination is A15, designated with an asterisk. (b) and (c) Chemical formulas for pteric acid and formycin 5'-monophosphate.

AMBER charges were used. Calculations of the electrostatic free energies were performed similar to those described above for the protein-RNA complex.

Of the remaining free energy terms in Eq. 1, we endeavored only to calculate the nonpolar contribution arising from the hydrophobic effect, using the following expression for the cavitation free energy (Jackson and Sternberg, 1994)

$$\Delta G_{\text{cav}} = \gamma \Delta A, \quad (6)$$

where ΔA is the change in the molecular surface area on complex formation and γ is the surface tension, initially set at 68 cal/mol/Å². This value of the surface tension was taken from a recent continuum analysis of an antibody-antibody complex and its 16 alanine substitutions (Olson, 1998).

Molecular surfaces were determined by the Connolly algorithm (Connolly, 1981) with a solvent probe radius set at 1.4 Å.

RESULTS AND DISCUSSION

We begin this section with an analysis of the absolute binding free energy for the RTA-RNA complex and its decomposition into individual amino acid residues on the protein interfacial surface and nucleotides on the RNA surface. This is followed by a discussion of calculations on small ligands.

Binding free energies for the RTA-RNA complex

Table 1 presents the results of Eq. 1 for the calculated total free energy of molecular association (ΔG_{calc}) for the wild-type protein and mutants Y80F, N209S, and R180Q, each interacting with the 29-mer RNA. Illustrated in Fig. 2 is the analyzed complex configuration, which was extracted from an ensemble of conformers generated by MD simulation methods (Olson, 1997). This configuration consists of a large network of molecular contacts where the target adenine base (designated as A15) of the GAGA hairpin structure is positioned in a recognition site between two tyrosine rings, one being the residue Tyr-80. The side chain of Asn-209 is hydrogen-bonded with the guanine base of G14, and Arg-180 contacts both the adenine base of A15 and the phosphate backbone linking the guanine G16. A putative catalytic water molecule is positioned in the active site near Arg-180 and was included explicitly in the treatment of the continuum description. Calculations on this specific conformer were carried out by using several different mean-field parameters describing the "macromolecule dielectric" and surface tension. The experimental binding free energy for the wild type was estimated from the expression $\Delta G_{\text{expt}} = -RT \ln K_m$, where K_m is the reported Michaelis constant (Kim and Robertus, 1992), and R is the universal gas constant. For the three mutants, relative changes in binding free energies were estimated from the reported K_m values and the catalytic rate constants (Kim and Robertus, 1992; Ready et al., 1991) by using an approximation that treats the kinetic off-rates as constant and much smaller than the corresponding turnover rates.

The first set of calculations applied parameter values of $\epsilon_m = 2$ and $\gamma = 68$ cal/mol/Å², where the dielectric constant is in the range of values commonly implemented in continuum models of protein-protein (e.g., Xu et al., 1997, and references cited therein) and protein-DNA interactions (Misra et al., 1994). Although both continuum parameter values appear to be reasonable, they are, nonetheless, somewhat arbitrary in their choice for constructing models of protein-nucleic acid interactions and serve only as initial estimates. Clearly an ϵ_m of 2 accounts only for electronic polarization and not the protein and solvent reorganization resulting from mutations. The value of ϵ_m can approach ~ 2 only when structural relaxation is explicitly taken into account (Sham et al., 1998; Warshel and Papazyan, 1998;

TABLE 1 Free energy terms (kcal/mol) for binding the 29-mer RNA substrate to ricin A-chain and single-residue mutants

Structure	$\Delta\Delta G_{\text{sol}}^{\text{prot-RNA}}$	$\Delta\Delta G_{\text{sol}}^{\text{RNA-prot}}$	ΔG_{int}	ΔG_{ele}	ΔG_{cav}	ΔG_{conf}^*	ΔG_{calc}	$\Delta G_{\text{expt}}^{\#}$
$\epsilon_m = 2$ and $\gamma = 68 \text{ cal mol}^{-1} \text{ \AA}^{-2}$								
Wild-type	72.6	143.2	-147.2	68.6	-95.5	16.3	-10.6	-9.0
Y80F	74.2	143.2	-146.7	70.7	-91.2	16.3	-4.2	-7.0
N209S	70.3	140.5	-141.7	69.1	-94.6	16.3	-9.2	-8.0
R180Q	74.9	139.7	-113.8	100.8	-93.7	16.3	23.4	-5.0
$\epsilon_m = 2.8$ and $\gamma = 68 \text{ cal mol}^{-1} \text{ \AA}^{-2}$								
R180Q	52.4	103.7	-83.0	73.1	-93.7	16.3	-4.3	-5.0
Scaled $\epsilon_m = \sim 7$ and $\gamma = \sim 20 \text{ cal mol}^{-1} \text{ \AA}^{-2}$								
Wild-type	20.5	40.3	-41.5	19.3	-28.1	0.0	-8.8	-9.0
Y80F	20.9	40.3	-41.3	19.9	-26.8	0.0	-6.9	-7.0
N209S	19.8	39.6	-39.9	19.5	-27.8	0.0	-8.3	-8.0
R180Q	21.1	39.4	-32.1	28.4	-27.6	0.0	0.8	-5.0
Scaled $\epsilon_m = \sim 9$ and $\gamma = \sim 20 \text{ cal mol}^{-1} \text{ \AA}^{-2}$								
R180Q	16.6	31.1	-25.3	22.4	-27.6	0.0	-5.2	-5.0

*Averaged conformational entropy and strain energy term fitted from ΔG_{expt} .

[#]Estimates of binding free energies using data reported by Robertus and co-workers (Kim and Robertus, 1992; Ready et al., 1990).

Muegge et al., 1998), and the simulated-annealing method used in deriving the RTA-RNA complex (Olson, 1997) achieved the relaxation needed for applying this dielectric value to the wild-type structure. However, and as described further below, the effect of reorganization for the mutants can be modeled implicitly by linearly scaling the free energy function.

The free energy term ΔG_{conf} in Table 1 represents the sum of conformational entropy and strain energy contributions, and the average of this term was estimated by empirically fitting the ΔG_{calc} for the wild-type structure and mutants Y80F and N209S to the ΔG_{expt} values. For this particular dielectric model, the mutant R180Q was eliminated in the numerical fit. The fitted ΔG_{conf} of ~ 16 kcal/mol is physically plausible given the size of the protein-RNA complex (Fig. 2 a). Theoretical estimates for protein-protein assemblies indicate that the rotational and translational entropy loss on complex formation is in the range of 2 to 15 kcal/mol at room temperature (Page and Jenks, 1971; Erickson, 1989; Finkelstein and Janin, 1989; Tidore and Karplus, 1994; Murphy et al., 1994). As for strain energies, values depend on the magnitude of induced fit and should be considerably less than the free energies of unfolding for both the unbound protein and RNA molecule. Further evaluations of the continuum model with ϵ_m set at 3 or higher yielded unrealistic values for ΔG_{conf} (depending, obviously, on the choice of γ), and thus suggest a reasonable a priori treatment of the electrostatics using an $\epsilon_m = 2$.

Notwithstanding the many caveats inherently built into the continuum model, the potential of mean force ($\Delta G_{\text{ele}} + \Delta G_{\text{cav}} \approx -27$ kcal/mol) plus a customary unfitted ΔG_{conf} estimate of ~ 15 kcal/mol (10 for entropic and 5 for strain energy; see, e.g., Froloff et al., 1997) yields a ΔG_{calc} for the wild-type assembly in good accord with ΔG_{expt} , which has an observed value of ~ -9 kcal/mol. The significance of this agreement is that the simulated-annealing method sampled conformational space sufficiently well in finding a conformer that represents an accurate description of the global binding mode of the rRNA substrate. The continuum

model reveals that ΔG_{int} is the largest free energy term, showing significant protein-RNA electrostatic interactions. This favorable term is, however, offset by the electrostatic desolvation cost of both molecules, particularly the RNA structure. The large penalty in desolvating the RNA is not unexpected and is the result of the negatively charged phosphate backbone involvement in the association process. An accurate treatment of the desolvation energetics for the RNA is critical in achieving a realistic total free energy of binding. A comparison of $\Delta\Delta G_{\text{sol}}^{\text{RNA-prot}}$ calculated by using the linearized Poisson-Boltzmann equation with the nonlinear form (Eq. 4) shows an increase of nearly 9 kcal/mol, which results in a significantly less favorable ΔG_{calc} .

Overall, our calculations indicate that the free energy terms describing the molecular association of the RTA protein with the RNA parallel those of protein-protein complexes, as analyzed by similar continuum approaches (Lee et al., 1992; Jackson and Sternberg, 1995; Froloff et al., 1997; Olson and Cuff, 1998; Olson, 1998; Muegge et al., 1998). Most importantly, the nonspecific hydrophobic effect provides the driving force underlying favorable complex formation ($\Delta G_{\text{cav}} = -95.5$ kcal/mol), while the net electrostatic contribution, with its role in conferring conformational specificity, opposes binding ($\Delta G_{\text{ele}} = +68.6$ kcal/mol). Our result of this balance between the hydrophobic effect and electrostatic specificity for the RTA-RNA complex is likely to be a generalization of proteins interacting with nucleic acids and simply extends earlier models of protein-protein association (e.g., Chothia and Janin, 1975), and the more recent analysis of ligand-DNA interactions (Misra and Honig, 1995). The magnitude of the predicted hydrophobic driving force in stabilizing RTA-RNA binding is reflected in a buried molecular surface area of $\sim 1400 \text{ \AA}^2$, which is comparable to large protein-protein interfaces. As described further below, the many contacts of this interface and their requisite for recognition and binding have important implications for the development of RTA inhibitors.

An improvement may be gained for Y80F in the relative free energy difference from the wild-type complex if the

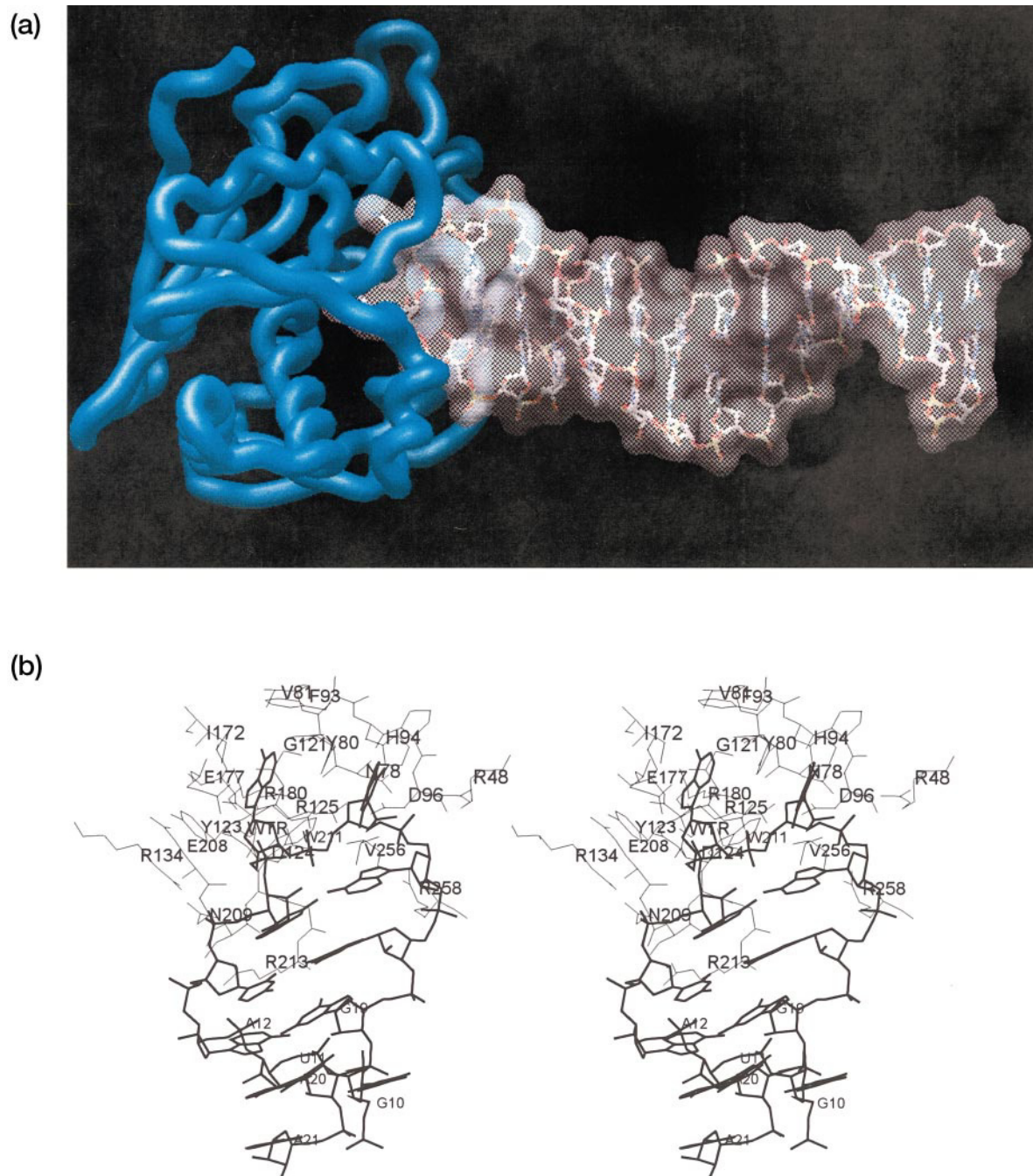


FIGURE 2 (a) Modeled complex between ricin A-chain (blue α -carbon trace) and the 29-mer oligonucleotide hairpin (molecular surface). (b) Stereoview of the bound active site of the protein-RNA complex, where the protein is illustrated by a thin line and the RNA loop structure as a thick line.

change in side-chain torsional freedom plays a favorable role in binding the rRNA substrate. The crystal structure of Y80F exhibits multiple side-chain conformations (Kim and Robertus, 1992), whereas the wild-type structure shows the tyrosine ring anchored by interactions of the hydroxyl group with the backbone of a neighboring active-site residue (Katzin et al., 1991; Rutenber et al., 1991). Co-crystal structures of RTA and several other RIPs bound with substrate analogs show disorder in the side chain of the tyrosine (Weston et al., 1994; Ren et al., 1994). Previous MD simulation anal-

ysis of the binding of ApG to RTA found similar conformational transitions for Tyr-80 (Olson, 1997). Although these observations suggest an entropic role for this residue and its phenylalanine substitution in binding the substrate, a full assessment of the side-chain conformational freedom is, nevertheless, difficult to estimate quantitatively by sampling active-site dynamics of both the unbound and bound states, and requires further study.

For the mutant R180Q, the putative catalytic water molecule was repositioned in the active site to bridge the

glutamine side chain with N3 of A15 (Day et al., 1996), and the resultant structure was subjected to a short MD simulation permitting structural relaxation. Despite these efforts, ΔG_{calc} shows a significant loss in free energy from the wild type. The ΔG_{ele} penalty can be reduced to obtain a more realistic ΔG_{calc} in better agreement with ΔG_{expt} by an increase in ϵ_m to a value set at ~ 2.8 , assuming the same fitted ΔG_{conf} . Using this dielectric constant yields a predicted $\Delta G_{\text{calc}} = -4.3$ kcal/mol (Table 1), which is in accord with $\Delta G_{\text{expt}} = -5$ kcal/mol. The requirement of a larger ϵ_m for modeling the mutation of a charged residue is not surprising, and it reflects the need for greater effective damping of the interactions within a dielectric continuum. In effect, scaling ϵ_m to larger values reduces the overestimation of both solvation and interaction energetics while avoiding the explicit reorganization of the pre-oriented dipoles found in the native complex (Sham et al., 1998; Warshel and Papayan, 1998; Muegge et al., 1997, 1998).

Assuming that ϵ_m is an adjustable parameter that represents the contributions that are not treated explicitly in continuum models, values of ΔG_{calc} corresponding to the wild-type and mutants Y80F and N209S can be reconciled with the experimental values if one readjusts ΔG_{ele} to reduce the overestimation of electrostatic energetics and absorbs the entropic term into ΔG_{cav} . The second set of calculations presented in Table 1 represents this empirical approach, which consists of free energies obtained from the following equation:

$$\Delta G_{\text{bind}} = \alpha \Delta G_{\text{ele}} + \beta \Delta G_{\text{cav}}, \quad (7)$$

where the α and β parameters are electrostatic and cavitation scaling factors, respectively, and are used to fit new values of ϵ_m and γ . Albeit this equation was evaluated as a mean-field model without thermal conformational sampling, it resembles a linear-response approximation (LRA) constructed with two free energy terms (Hansson et al., 1998, and references cited therein). A minor difference with LRA is the choice of the nonpolar term (for an exception, see Lee et al., 1992), where we strictly used the solvent cavitation free energy, and by means of an enthalpy-entropy compensation argument (Nicholls et al., 1991; Jackson and Sternberg, 1994, 1995), we neglected the van der Waals interactions. As will be shown below, the underlying purpose of linearly scaling the free energies is to provide a calculational framework where small ligands, and presumably large RNA-based inhibitors (Chen et al., 1996), can be directly compared against the rRNA substrate while avoiding the complexities of estimating ΔG_{conf} . Continuum parameters for this model were fitted to ΔG_{expt} and yielded a larger ϵ_m value of ~ 7 and a lower γ of ~ 20 cal/mol/Å², where the surface tension is now more characteristic of “microscopic” values used with modeling solvent-accessible surfaces (Jackson and Sternberg, 1994). Both parameters are “physically” reasonable and are consistent with the spirit of implicit models. The errors in ΔG_{calc} and in the relative free energy changes are significantly reduced, while

R180Q still requires a larger ϵ_m value of ~ 9 to achieve an agreement with ΔG_{expt} . The hydrophobic effect remains the driving force for complex formation, although ΔG_{cav} now represents an effective free energy term depending on more than molecular complementarity.

Decomposition of binding free energy

The free energy terms ΔG_{ele} and ΔG_{cav} calculated above represent an aggregate of many contributions at the binding interface between RTA and the RNA, which can be decomposed on a per-residue level into individual contributions arising from both molecules. Various calculational schemes are available for dissecting binding free energies, the most notable being the recent methods developed and applied by Warshel and co-workers (Muegge et al., 1996–1998). Here, for electrostatics of the protein, atomic charges were switched on and off one residue at a time for interfacial side chains within 3.5 Å of the RNA molecule. Electrostatics of the backbone and the protein outside of the interface were treated as part of the remaining aggregate. The hydrophobic effect was decomposed by using a per-residue buried molecular surface area. Similar calculations were conducted for the RNA, except the CGAGAG loop region was dissected in terms of structural groups corresponding to the bases, phosphate groups, and ribose rings. Combined, the sum of individual contributions of each molecule assures a complete thermodynamic cycle and provides an efficient approach of gauging residue contributions to molecular association without the computational task of evaluating free energies arising from mutations. Although this approach is more efficient, a direct comparison with site-directed mutagenesis is only an approximation. Nevertheless, it is likely that the *relative ranking* of these artificial mutants correlates well with experimental measurements using glycine substitutions of the protein interacting with, for example, the 14-mer ribonucleotide transition-state mimic inhibitor (Chen et al., 1996), or a 29-mer RNA hairpin with the catalytic adenine replaced with a nonhydrolyzable complementary ring.

Summarized in Table 2 are the key contributions for RTA residues interacting with the RNA molecule calculated by using the scaled parameters $\epsilon_m = 7.1$ and $\gamma = 20.0$ cal/mol/Å² to evaluate the continuum model. Similar qualitative results are obtained using $\epsilon_m = 2$ and $\gamma = 68$ cal/mol/Å² with the entropic factor included. Alternatively, Warshel and co-workers (Muegge et al., 1997, 1998) suggested the use of a priori ϵ_m values of 4 and 20 for uncharged and charged residues, respectively, in their studies of dissecting the free energies of protein complexes, although they neglected the cavitation energetics. The components of ΔG_{calc} are now defined for contact residues (ΔG_{res}), where $\Delta \Delta G_{\text{sol}}$ is the desolvation of RTA side chains upon binding the RNA, ΔG_{int} is the corresponding residue side-chain electrostatic interaction, and ΔG_{cav} is the effective contribution of the total residue to the net cavitation energy. Illustrated in Fig. 3 are values for ΔG_{ele} and ΔG_{cav} projected onto the

TABLE 2 Key ricin A-chain residue side-chain contributions (kcal/mol) to binding the 29-mer RNA substrate

Residue	$\Delta\Delta G_{\text{sol}}^{\text{prot-RNA}}$	$\Delta G_{\text{int}}^{\text{prot-RNA}}$	ΔG_{ele}	ΔG_{cav}	ΔG_{res}
R48	1.6	-6.1	-4.5	-0.4	-4.9
N78	0.4	-0.9	-0.5	-0.8	-1.3
Y80	0.2	-0.4	-0.2	-1.6	-1.8
V81	0.0	-0.1	-0.1	-0.4	-0.5
D96	1.3	0.6	1.9	-0.5	1.4
N122	0.9	-3.6	-2.7	-1.0	-3.7
Y123	0.1	-1.9	-1.8	-1.2	-3.0
D124	0.4	3.1	3.5	-0.2	3.3
R125	0.1	-2.1	-2.1	-0.1	-2.2
R134	1.5	-10.2	-8.7	-0.3	-9.0
I172	0.0	-0.2	-0.2	-0.9	-1.1
E177	2.6	7.3	9.9	-0.3	9.6
R180	3.7	-12.4	-8.7	-0.6	-9.3
E208	1.4	5.7	7.1	-0.5	6.6
N209	0.4	-2.3	-1.9	-1.0	-2.9
W211	0.0	0.1	0.1	-0.6	-0.5
R213	4.7	-19.7	-15.0	-1.5	-16.5
R258	2.5	-13.7	-11.2	-0.6	-11.8

protein molecular surface (Nicholls et al., 1991). Surfaces colored red depict “hot” residues that contribute significantly to the favorable RNA association, whereas dark blue-colored surfaces are “cold” residues that destabilize the binding. The bound ligand shown is the target adenine of the 29-mer RNA hairpin.

The decomposed ΔG_{calc} indicates significant stabilization to the RNA association arising from the positively charged arginines located in the active-site cleft. These solvent-exposed residues easily offset their desolvation penalties, allowing favorable ΔG_{ele} values to provide electrostatic complementarity to the negatively charged RNA phosphate backbone, which is characterized by a much greater desolvation cost. Several residues of this arginine-rich binding motif are either invariant or conserved among the RIPs. The

two most favorable contributing residues, Arg-213 and Arg-258, function by anchoring the phosphate backbone of the Watson-Crick basepair of C13 and G18, which closes the loop structure of the RNA hairpin (Fig. 2 *b*). Arg-213 is conserved, showing a positive charge in nearly 60% of the RIPs, while Arg-258 is highly variable and may be responsible, in part, for differentiating the binding affinities among the RIPs for the substrate. An additional possible significance of these two arginines is that their high affinities may “unzip” the basepairs in RNA ligands with short stems (Link et al., 1995), leading to the lack of inhibition. Further contributions to this RNA molding are likely to arise from arginines 48 and 134, with the former residue variable and the latter invariant. The side chain of Arg-134 contributes significantly to substrate specificity through electrostatic interactions with the base of G14.

The calculations also indicate that in contrast to the arginines, all of the negatively charged residues in contact with the RNA produce unfavorable ΔG_{ele} contributions. These electrostatic values, ranging from ~ 2 to 9 kcal/mol, clearly depend on the choice of ionization state for each asparagine and glutamate. The net destabilization effect of these negative charges is conceivably the energetic cost of providing a network of charge-charge balance needed in stabilizing the tertiary structure of the unbound active-site cleft (Day et al., 1996; Kim and Robertus, 1992). For example, disrupting the ion pair between Glu-177 and Arg-180 by replacing the arginine with a histidine affects the global stability of RTA if the imidazole ring is deprotonated (Day et al., 1996). Further mutagenesis can be suggested from our electrostatic calculations, particularly substitutions of many of the high-affinity arginines and several of their hydrophilic bridges in the active site with hydrophobic isosteres (Hendsch and Tidor, 1994), thus predicting a stable protein yet weaker binding complex. The particularly large unfavorable contribution from the invariant Glu-177

FIGURE 3 Functional-interaction surface predicted for ricin A-chain interacting with the 29-mer oligonucleotide hairpin. On the left, the net electrostatic free energy (ΔG_{ele}) dissected per residue side chain for ricin A-chain contribution projected onto its protein molecular surface, and similarly on the right, the solvent cavitation free energy (ΔG_{cav}). The free energy scale (kcal/mol) is as follows: color red, free energy contributions ≤ -3 ; $-3 < \text{yellow} \leq -2$; $-2 < \text{green} \leq -1$; $-1 < \text{cyan} \leq +1$; blue $> +1$. Shown is the target adenine of the 29-mer RNA hairpin for depurination.

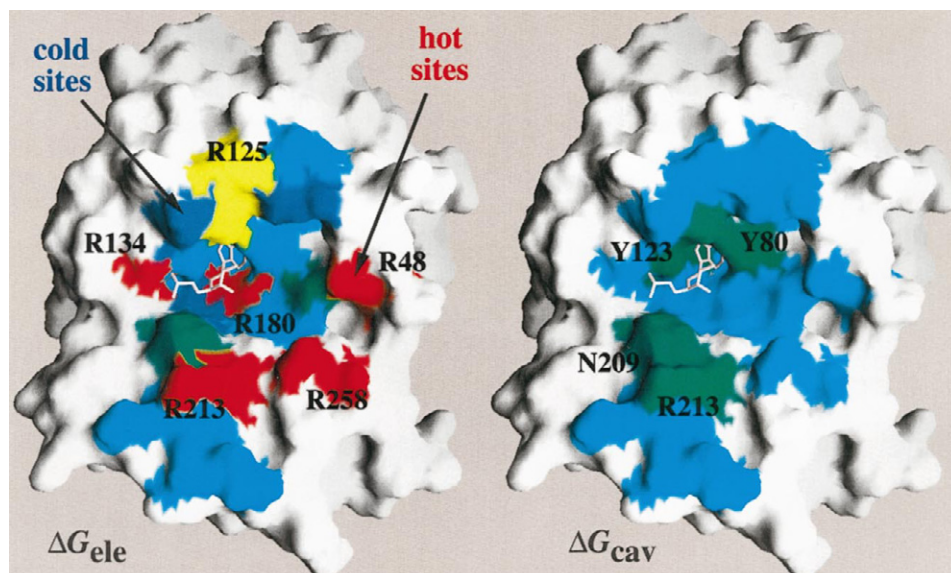


TABLE 3 Key contributions (kcal/mol) of the 29-mer RNA substrate to binding ricin A-chain

Nucleotide	$\Delta\Delta G_{\text{sol}}^{\text{RNA-prot}}$	$\Delta G_{\text{int}}^{\text{RNA-prot}}$	ΔG_{ele}	ΔG_{cav}	ΔG_{res}
Bases					
C13	0.1	0.6	0.1	-0.2	0.5
G14	0.9	-2.7	-1.8	-1.1	-2.9
A15	1.4	-0.6	0.8	-2.6	-1.8
G16	1.3	-0.9	0.4	-1.7	-1.3
A17	0.1	-0.4	-0.3	-0.1	-0.4
G18	0.2	-0.4	-0.2	-0.1	-0.3
Phosphate groups					
C13	2.7	-5.8	-3.1	-0.2	-3.3
G14	3.8	-7.0	-3.2	-0.5	-3.7
A15	7.0	-5.4	1.6	-0.6	1.0
G16	6.4	-6.7	-0.3	-0.4	-0.7
A17	5.5	-9.2	-3.7	-0.7	-4.4
G18	1.5	-5.2	-3.7	-0.3	-4.0
Ribose rings					
C13	0.1	-0.1	0.0	-0.1	-0.1
G14	0.2	0.1	0.3	-0.3	0.0
A15	1.1	0.0	1.1	-1.2	-0.1
G16	0.5	0.0	0.5	-0.8	-0.3
A17	0.1	0.0	0.1	-0.1	0.0
G18	0.0	-0.2	-0.2	0.0	-0.2

near the target adenine may also help stabilize the charge distribution of the transition-state complex.

Hydrophobic effects appear diffuse across the large interfacial area (Fig. 3), showing an average per residue ΔG_{cav} of ~ -0.5 kcal/mol. Two clusters of residues exhibiting larger values are the tyrosines 80 and 123, and the cluster of Asn-209 and Arg-213. The complementary ΔG_{res} values for the RNA hexamer loop region, dissected per nucleotide, are presented in Table 3. Nearly half of the net RNA cavitation energy of ~ -14 kcal/mol is contributed by the tetraloop base structure, and the phosphoribose backbone contributes slightly less. The calculations indicate that stacking A15 between the tyrosines together with stacking G16 in a recognition site on the opposite side of Tyr-80 (Fig. 2 b) forms a compacted hydrophobic core with comparatively low desolvation energetics, reminiscent of protein folding.

In terms of electrostatic specificity, only the base of G14 can easily balance its desolvation penalty, showing a $\Delta G_{\text{ele}} = -1.8$ kcal/mol. The guanine base forms hydrogen bonds with Asn-209 and Arg-213, and the pair-wise ΔG_{int} for these two interactions are calculated to have affinities of -0.8 and -2.6 kcal/mol, respectively. Although both hydrophilic interactions are favorable, neither is sufficiently

strong to compensate for their desolvation cost in stabilizing complex formation (from Tables 2 and 3, $\Delta\Delta G_{\text{sol}}$ of 1.3 kcal/mol for the N209-G14 interaction and 5.6 kcal/mol for R213-G14). Rather, the calculations show that G14 is buried in a favorable electrostatic environment of surrounding protein residues, and similarly, the two RTA side chains are buried in an RNA environment that allows binding to occur. A continuum analysis of hydrophilic bridges for protein-protein complexes suggests similar favorable energetic roles in stabilizing complex formation (Xu et al., 1997). The specific interactions of the A15 base is balanced by favorable and unfavorable contributions arising from Arg-180 and Glu-177, plus backbone interactions of Val-81 and Gly-121 in the aggregate contribution. The larger desolvation cost of A15 and G16 relative to the other bases is a result of the unstacking and rotation of both nucleotides from their initial positions found in the unbound NMR structure (Szewczak and Moore, 1995).

RNA binding is dominated by the nonspecific interactions of the phosphate backbone. Net electrostatic contributions (ΔG_{ele}) from the backbones of A15 and G16 are weak, while the flanking nucleotides exhibit favorable energetics. Again, this effect is a function of the perturbation placed on rotating the reverse turn of the hairpin, resulting from the electrostatic complementarity of the active-site cavity. Contributions arising from the ribose groups are minimal for this particular RNA conformer in binding the protein.

Binding free energies for small ligands

Presented in Table 4 are the ΔG_{calc} values for ligands PTA, FMP, and ApG, bound to the active site of RTA. Calculations of the NLPB equation were carried out with continuum parameter values set at $\epsilon_m = 7.1$ and $\gamma = 20.0$ cal/mol/Å², as used in the free energy decomposition of the RTA-RNA assembly. The FMP binding free energy was calculated for three different structures, where the first two used the x-ray crystallographic complex (Monzingo and Robertus, 1992) and modeled the phosphate group as a monoanion and dianion. The third structure was taken from a previously reported MD simulation of the dianion ligand with RTA (Olson et al., 1995).

The calculations indicate that for PTA and ApG, the free energies of binding reproduced the estimated ΔG_{expt} values within ± 1 kcal/mol. Similar calculations, using $\epsilon_m = 2$ and $\gamma = 68$ cal/mol/Å², yielded overestimates of favorable

TABLE 4 Free energy terms (kcal/mol) for binding small ligands to the active site of ricin A-chain

Structure	$\Delta\Delta G_{\text{sol}}^{\text{prot-lig}}$	$\Delta\Delta G_{\text{sol}}^{\text{lig-prot}}$	$\Delta G_{\text{int}}^{\text{prot-lig}}$	ΔG_{ele}	ΔG_{cav}	ΔG_{calc}	ΔG_{expt}^*
PTA	4.3	6.9	-6.4	4.8	-8.4	-3.6	-4.4
FMP (-1)	4.8	6.3	-4.0	7.1	-6.8	0.3	~ -3
FMP (-2)	4.8	5.1	-3.5	6.4	-6.8	-0.4	~ -3
sim-FMP (-2)	5.3	6.9	-5.4	6.8	-9.0	-2.2	~ -3
ApG	3.7	5.3	-2.0	7.0	-10.5	-3.5	~ -3

*Estimates of binding free energies using data reported by Robertus and co-workers (Yan et al., 1997; Monzingo and Robertus, 1992). The number in parentheses for FMP denotes the formal charge of either a monoanion or dianion, and sim-FMP represents the MD simulation structure (Olson et al., 1995).

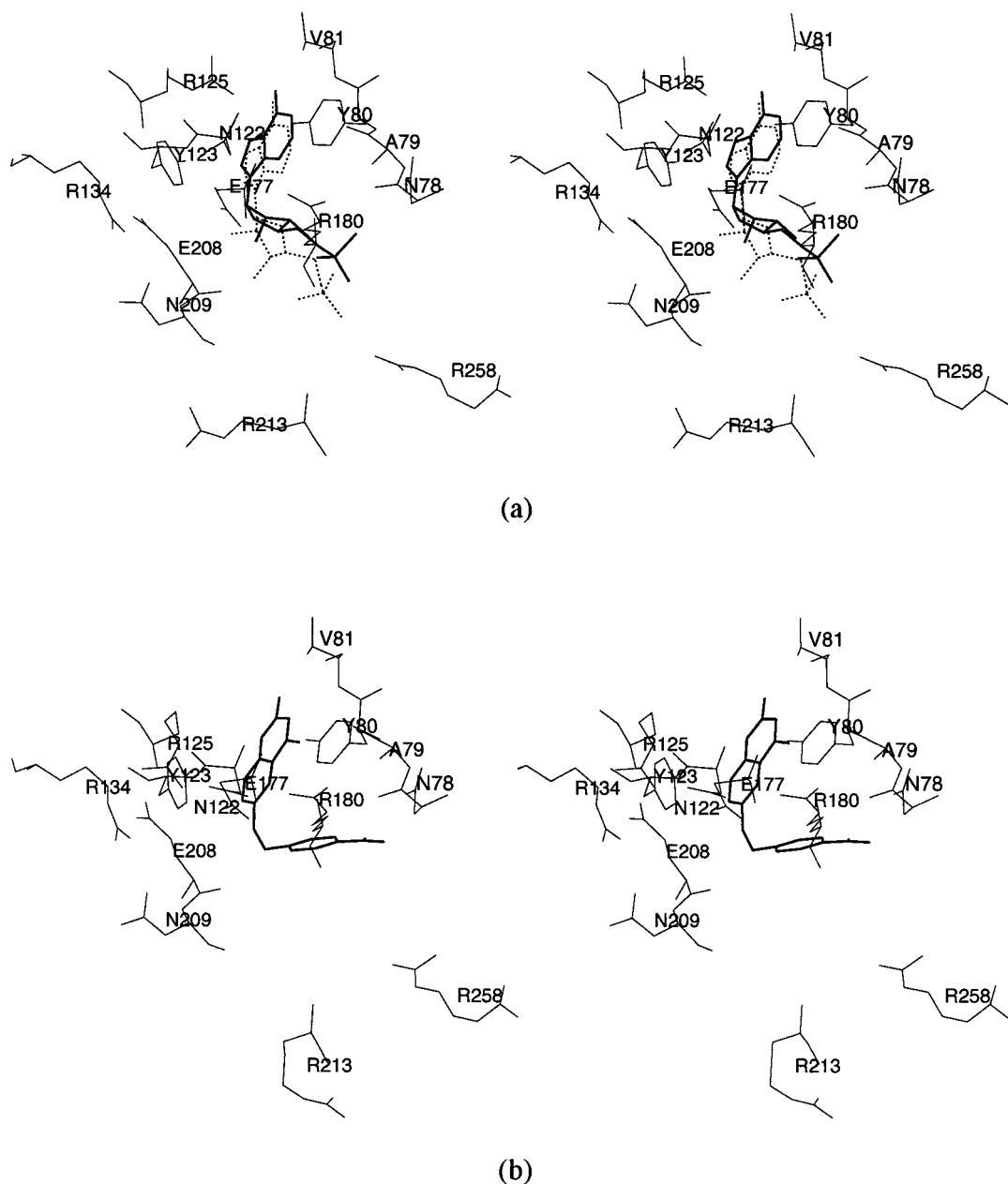


FIGURE 4 (a) Stereoview of formycin 5'-monophosphate bound in the ricin A-chain active site. Ligand crystal structure is shown as a thick line and the molecular-dynamics simulation structure (Olson et al., 1995) is depicted as a dashed line. Protein residues are shown as thin lines. (b) Stereoview of the crystal structure of pteric acid (*thick line*) bound to ricin A-chain (*thin line*).

binding, and thus require various assumptions regarding entropic costs. As mentioned above, the ansatz of absorbing the ΔG_{conf} term for the RNA complex into the continuum description permits direct comparisons with the binding of small ligands (described further below). For ligand molecules it has generally been argued, based on crystallographic thermal factors and mean-free paths, that the configurational volumes for translational freedom do not differ appreciably between the bound and free states (Murphy et al., 1994). Nevertheless, cratic entropy resulting from mixing may lead to free energy penalties estimated at 2 kcal/mol for molecular association at room temperature (Murphy et al.,

1994). Many empirical studies of binding small ligands to proteins apply either ad hoc values for translational and rotational entropy of 1 to 2 kcal/mol, or simply neglect the contribution altogether. In either case, the ΔG_{calc} values using $\epsilon_m = 7.1$ and $\gamma = 20.0$ cal/mol/Å² appear to be good estimates of ligand binding.

For calculations on FMP, analysis of the crystal structure modeled either as a monoanion or dianion ligand yielded values of ΔG_{calc} showing large errors, while the simulation structure for the dianion reveals a much better agreement. A possible explanation of this variance may lie in differences of the binding thermodynamics found in the crystal and in

aqueous solution. The more favorable interaction energy of the simulation structure results from an ion-pair interaction of the phosphate group with Arg-258 (Fig. 4 *a*); an interaction similar to those dominating the RNA binding. Concomitantly, this repositioning of the phosphate group accounts for the larger desolvation costs of both the protein and ligand. The increase in ΔG_{cav} is due to the overall optimization of the complex, in particular, packing of the formycin ring between tyrosines 80 and 123.

A comparison of the free energy terms governing the binding of the ligands with those of the 29-mer RNA using the same continuum parameter set (see Table 4 versus Table 1) clearly shows the task at hand in designing small inhibitors that effectively compete for the active site of RTA. As expected, the individual energetics for each of the terms are significantly reduced for the ligands. For example, the cavitation energies are nearly 20 kcal/mol less stable, and similarly, the electrostatic interactions are weaker by more than 30 kcal/mol. What is important, however, as found for the native protein-RNA complex, is the minimization of ΔG_{ele} and its offset achieved by optimizing ΔG_{cav} . The ligand PTA exhibits the most favorable ΔG_{ele} , while ApG shows the largest buried surface area for determining ΔG_{cav} . Neither of the two ligands attracts many of the critical binding points found stabilizing the rRNA substrate, which appear scattered across the large buried surface area (see Fig. 3). Decomposition of ΔG_{calc} for the RTA-PTA complex (Table 5) shows Arg-180 making favorable contributions to ΔG_{ele} , while many of the arginines predicted in binding the 29-mer RNA contribute very little.

Our calculations for contrasting the small ligands with the large RNA molecule suggest that an analysis of the key chemical groups in the active site that interact with the substrate should be useful in the design of effective inhibitors by focusing on chemical moieties accessible to the ligands. For example, possible improvement in the binding affinity of PTA may be gained by extending the size of the ligand to take advantage of charge-charge interactions with Arg-258 (Fig. 4 *b*), although the desolvation penalty must

be carefully minimized for both the ligand and protein. Alternatively, the ΔG_{ele} surface of Fig. 3 indicates regions remote from the adenine binding site that may provide sufficient nucleation sites to “grow” small molecules with optimized favorable free energies. The calculations on PTA also reveal that the cavitation energies of tyrosines 80 and 123 confer critical nonspecific interactions with the pterin ring, albeit less than those observed in the packing of A15 and G16 for the RNA complex. Improvement in this particular hydrophobic binding may be difficult without creating large branched ligands (note ApG lacks conformational mimicry with the binding of G16). As was predicted for the RTA-RNA complex, negatively charged residues destabilize the binding of PTA.

Finally, a unified model for RTA binding of the rRNA substrate and small ligands was constructed by fitting Eq. 7. Free energy terms for ΔG_{ele} and ΔG_{cav} for RTA and mutants Y80F and N209S were taken from Table 1, and values for ligands PTA, FMP (simulation), and ApG from Table 4. Fitting these six structures yielded an $\epsilon_m = 6.4$ and $\gamma = 21.5$ cal/mol/Å², and a scatter plot of ΔG_{calc} versus ΔG_{expt} using these values is presented in Fig. 5. Although the data set is relatively small, the quality of the fit yields a correlation coefficient of 0.9 and an estimated average absolute error of ± 0.5 kcal/mol. The improved agreement for the small ligands (Table 4 versus Fig. 5) is the result of including the RNA complex into the fitted continuum parameters, and may reflect the fact that the binding is dominated by the larger and more stable complex. Difficulties can typically arise for modeling small ligands because of their weaker binding affinities and, moreover, possible multiple binding modes. The lack of these problems in the RTA-RNA complex contributes significantly to the success of modeling the

TABLE 5 Ricin A-chain residue side-chain contributions (kcal/mol) to binding pterioic acid

Residue	$\Delta\Delta G_{\text{sol}}^{\text{prot-RNA}}$	$\Delta G_{\text{int}}^{\text{prot-RNA}}$	ΔG_{ele}	ΔG_{cav}	ΔG_{res}
R48	0.0	-0.5	-0.5	0.0	-0.5
N78	0.2	-0.8	-0.6	-0.4	-1.0
Y80	0.0	-0.2	-0.2	-0.8	-1.0
V81	0.0	0.0	0.0	-0.3	-0.3
N122	0.0	-0.1	-0.1	-0.1	-0.2
Y123	0.0	0.0	0.0	-0.7	-0.7
R125	0.0	-0.1	-0.1	0.0	-0.1
R134	0.1	-0.2	-0.1	0.0	-0.1
I172	0.0	-0.1	-0.1	-0.6	-0.7
E177	2.9	1.4	4.3	-0.2	4.1
R180	3.1	-4.4	-1.3	-0.6	-1.9
E208	0.2	0.5	0.7	-0.3	0.4
W211	0.0	0.0	0.0	-0.6	-0.6
R213	0.0	-0.1	-0.1	0.0	-0.1
R258	0.0	-0.7	-0.7	0.0	-0.6

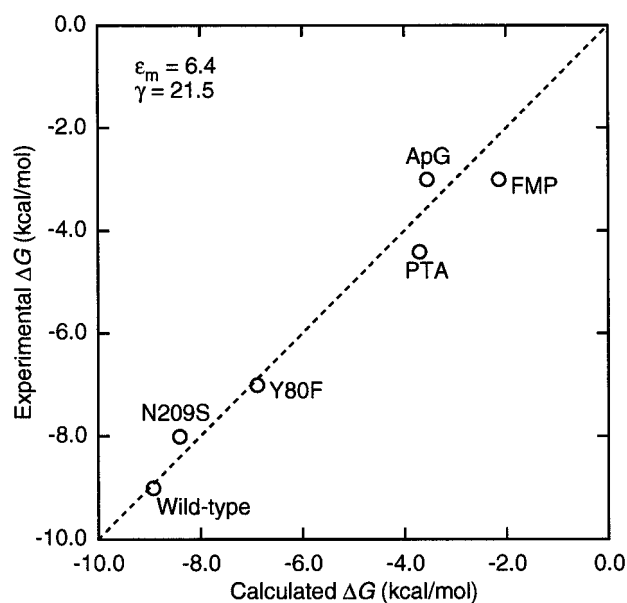


FIGURE 5 Scatter plot of ΔG_{calc} versus ΔG_{expt} for a continuum model parametrized for both the RNA substrate and small ligand molecules.

mutations and, in general, the continuum modeling of macromolecular complexes.

It is noteworthy that this linear scaling of a protein and several variants binding its large substrate, combined with scaling of small ligands complexed to the same native protein, is unique among continuum analyses of molecular association. The utility of unifying the continuum parameters allows putative ligands found either by de novo design methods or database searching to be scored against the substrate based on free energies, rather than the naive and futile evaluations of structural-interaction energies via atomic force-fields. Although this particular point is well known among the molecular docking community, the calculations presented here clearly demonstrate the significance of having an empirical approach, which incorporates a realistic thermodynamic description of binding and which is suitable for modifying ligands to improve their affinities. These goals are not unique and are similar with recent reported applications of the LRA (e.g., Jones-Hertzog and Jorgensen, 1997), albeit solutions to Eq. 7, and in particular, the NLPB equation, provide a mean-field approach. It remains to be seen if this continuum model yields any "universality" in the parameters ϵ_m and γ for gauging the binding affinities of the other RIPs with the 29-mer RNA and small substrate analogs.

We thank A. F. Monzingo and J. D. Robertus for making the crystallographic structures available. We gratefully acknowledge the Biomedical Supercomputing Center of the Frederick Cancer Research and Development Center for a generous grant of computer time.

The work of L.C. was supported by the Army High Performance Computing Research Center under the auspices of the Department of the Army, Army Research Laboratory cooperative agreement number DAAH04-95-2-0003/contract number DAAH04-95-C-0008.

REFERENCES

- Chen, X. Y., T. Link, and V. L. Schramm. 1996. Inhibition of ricin by an RNA stem-loop containing a ribo-oxocarbenium mimic. *J. Am. Chem. Soc.* 118:3067–3068.
- Chothia, C. H., and J. Janin. 1975. Principles of protein-protein recognition. *Nature*. 256:705–708.
- Connolly, M. L. 1981. Molecular surface program 429. The quantum chemistry program exchange, Indiana University, Bloomington, Indiana 47405, USA.
- Day, P. J., S. R. Ernst, A. E. Frankel, A. F. Monzingo, J. M. Pascal, M. C. Molina-Svinth, and J. D. Robertus. 1996. Structure and activity of an active site substitution of ricin A chain. *Biochemistry*. 35:11098–11103.
- Erickson, H. P. 1989. Co-operativity in protein-protein association: the structure and stability of the actin filament. *J. Mol. Biol.* 206:465–474.
- Finkelstein, A. V., and J. Janin. 1989. The price of lost freedom: entropy of biomolecular complex formation. *Protein Eng.* 3:1–3.
- Frankel, A., P. Welsh, J. Richardson, and J. D. Robertus. 1990. The role of arginine 180 and glutamic acid 177 of ricin toxin A chain in the enzymatic inactivation of ribosomes. *Mol. Cell. Biol.* 10:6257–6263.
- Froloff, N., A. Windemuth, and B. Honig. 1997. On the calculation of binding free energies using continuum methods: application to MHC class I protein-peptide interactions. *Protein Sci.* 6:1293–1301.
- Gilson, M. K., and B. Honig. 1988. Calculation of the total electrostatic energy of a macromolecular system: solvation energies, binding energies, and conformational analysis. *Proteins*. 4:7–18.
- Gilson, M. K., K. A. Sharp, and B. Honig. 1988. Calculating the electrostatic potential of molecules in solution: method and error assessment. *J. Comput. Chem.* 9:327–335.
- Hansson, T., J. Marelus, and J. Åqvist. 1998. Ligand binding affinity prediction by linear interaction energy methods. *J. Comput. Aided Mol. Des.* 12:27–35.
- Hendsch, Z. S., and B. Tidor. 1994. Do salt bridges stabilize proteins? A continuum electrostatic analysis. *Protein Sci.* 3:211–226.
- Jackson, R. M., and M. J. E. Sternberg. 1994. Application of scaled particle theory to model the hydrophobic effect: implications for molecular association and protein stability. *Protein Eng.* 7:371–383.
- Jackson, R. M., and M. J. E. Sternberg. 1995. A continuum model for protein-protein interactions: application to the docking problem. *J. Mol. Biol.* 250:258–275.
- Jayaram, B., K. A. Sharp, and B. Honig. 1989. The electrostatic potential of DNA. *Biopolymers*. 28:975–993.
- Jones-Hertzog, D. K., and W. L. Jorgensen. 1997. Binding affinities for sulfonamide inhibitors with human thrombin using Monte Carlo simulations with a linear response method. *J. Med. Chem.* 40:1539–1549.
- Jorgensen, W. L., J. Chandrasekhar, J. D. Madura, R. W. Impey, and M. L. Klein. 1983. Comparison of simple potential functions for simulation of liquid water. *J. Chem. Phys.* 79:926–935.
- Katzin, B. J., E. J. Collins, and J. D. Robertus. 1991. The structure of ricin A-chain at 2.5 Å. *Proteins*. 10:251–259.
- Kim, Y. S., and J. D. Robertus. 1992. Analysis of several key active site residues of ricin A chain by mutagenesis and x-ray crystallography. *Protein Eng.* 5:775–779.
- Lee, F. S., Z. T. Chu, M. B. Bolger, and A. Warshel. 1992. Calculations of antibody-antigen interactions: microscopic and semi-microscopic evaluation of the free energies of binding of phosphorylcholine analogs to McPC603. *Protein Eng.* 5:215–228.
- Link, T., X. Y. Chen, L. H. Niu, and V. L. Schramm. 1995. Ricin A-chain activity and inhibitor studies with oxycarbenium analogues. *FASEB*. 9:A1423.
- Maple, J. R., M.-J. Hwang, T. P. Stockfisch, U. Dinur, M. Walkdman, C. S. Ewig, and A. T. Hagler. 1994. Derivation of class II force fields. 1. Methodology and quantum force field for the alkyl functional group and alkane molecules. *J. Comput. Chem.* 15:195–231.
- Misra, V. K., J. L. Hecht, K. A. Sharp, R. A. Friedman, and B. Honig. 1994. Salt effects on protein-DNA interactions. The λ cl repressor and EcoRI endonuclease. *J. Mol. Biol.* 238:264–280.
- Misra, V. K., and B. Honig. 1995. On the magnitude of the electrostatic contribution to ligand-DNA interactions. *Proc. Natl. Acad. Sci. USA*. 92:4691–4695.
- Monzingo, A. F., and J. D. Robertus. 1992. X-ray analysis of substrate analogs in the ricin A-chain active site. *J. Mol. Biol.* 227:1136–1145.
- Muegge, I., T. Schweins, R. Langen, and A. Warshel. 1996. Electrostatic control of GTP and GDP binding in oncoprotein p21^{ras}. *Structure*. 4:475–489.
- Muegge, I., T. Schweins, and A. Warshel. 1998. Electrostatic contributions to protein-protein binding affinities: application to Rap/Raf interaction. *Proteins*. 30:407–423.
- Muegge, I., H. Tao, and A. Warshel. 1997. A fast estimate of electrostatic group contributions to the free energy of protein-inhibitor binding. *Protein Eng.* 10:1363–1372.
- Murphy, K. P., D. Xie, K. S. Thompson, L. M. Amzel, and E. Freire. 1994. Entropy in biological binding processes: estimation of translational entropy loss. *Proteins*. 18:63–67.
- Nicholls, A., and B. Honig. 1991. A rapid finite difference algorithm, utilizing successive over-relaxation to solve the Poisson-Boltzmann equation. *J. Comput. Chem.* 12:435–445.
- Nicholls, A., K. A. Sharp, and B. Honig. 1991. Protein folding and association: insights from the interfacial and thermodynamic properties of hydrocarbons. *Proteins*. 11:281–296.
- Olson, M. A. 1997. Ricin A-chain structural determinant for binding substrate analogues: a molecular dynamics simulation analysis. *Proteins*. 27:80–95.
- Olson, M. A. 1998. Mean-field analysis of protein-protein interactions. *Biophys. Chem.* (in press).

- Olson, M. A., and L. Cuff. 1998. Molecular docking of superantigens with class II major histocompatibility complex proteins. *J. Mol. Recogn.* 10:277–289.
- Olson, M. A., J. P. Scovill, and D. C. Hack. 1995. Simulation analysis of formycin 5'-monophosphate analog substrates in the ricin A-chain active site. *J. Comput. Aided Mol. Des.* 9:226–236.
- Page, M. I., and W. P. Jenks. 1971. Entropic contribution to rate acceleration in enzymic and intramolecular reactions and the chelate effect. *Proc. Natl. Acad. Sci. USA.* 68:1678–1683.
- Ready, M. P., Y. S. Kim, and J. D. Robertus. 1991. Directed alteration of active site residues in ricin A chain and implications for the mechanism of action. *Proteins.* 10:270–278.
- Reiner, E. S., and C. J. Radke. 1990. Variational approach to the electrostatic free energy in charged colloidal suspensions: general theory for open systems. *J. Chem. Soc. Faraday Trans.* 86:3901–3912.
- Ren, J., Y. Wang, Y., Dong, and D. I. Stuart. 1994. The *N*-glycosidase mechanism of ribosome-inactivating proteins implied by crystal structures of α -momorcharin. *Structure.* 2:7–16.
- Rutenber, E., B. J. Katzin, E. J. Collins, D. Mlsna, S. E. Ernst, M. E. Ready, and J. D. Robertus. 1991. The crystallographic refinement of ricin at 2.5 Å resolution. *Proteins.* 10:240–250.
- Sham, Y. Y., I. Muegge, and A. Warshel. 1998. The effect of protein relaxation on charge–charge interactions and dielectric constants of proteins. *Biophys J.* 74:1744–1753.
- Sharp, K. A., and B. Honig. 1990. Calculating total electrostatic energies with the nonlinear Poisson-Boltzmann equation. *J. Phys. Chem.* 94: 7684–7692.
- Szewczak, A. A., and P. B. Moore. 1995. The sarcin/ricin loop, a modular RNA. *J. Mol. Biol.* 247:81–98.
- Szewczak, A. A., P. B. Moore, Y.-L. Chan, and I. G. Wool. 1993. The conformation of the sarcin/ricin loop from 28S ribosomal RNA. *Proc. Natl. Acad. Sci. USA.* 90:9581–9585.
- Tidor, B., and M. Karplus. 1994. The contribution of vibrational entropy to molecular association. *J. Mol. Biol.* 238:405–414.
- Warshel, A., and A. Papazyan. 1998. Electrostatic effects in macromolecules: fundamental concepts and practical modeling. *Curr. Opin. Struct. Biol.* 8:211–217.
- Weiner, S. J., P. A. Kollman, D. T. Nguyen, and D. A. Case. 1986. An all atom forcefield for simulations of proteins and nucleic acid. *J. Comput. Chem.* 7:230–252.
- Weston, S. A., A. D. Tucker, D. R. Thatcher, D. J. Derbyshire, and R. A. Pauptit. 1994. X-ray structure of recombinant ricin A-chain at 1.8 Å resolution. *J. Mol. Biol.* 244:410–422.
- Xu, D., S. L. Lin, and R. Nussinov. 1997. Protein binding versus protein folding: the role of hydrophilic bridges in protein associations. *J. Mol. Biol.* 265:68–84.
- Yan, X., P. Day, T. Hollis, A. F. Monzingo, E. Schelp, J. D. Robertus, G. W. A. Milne, and S. Wang. 1998. Recognition and interaction of small rings with the ricin A-chain binding site. *Proteins.* 31:33–41.
- Yan, X., T. Hollis, M. Svinth, P. Day, A. F. Monzingo, G. W. A. Milne, and J. D. Robertus. 1997. Structure-based identification of a ricin inhibitor. *J. Mol. Biol.* 266:1043–1049.